Chemical Science

ROYAL SOCIETY OF CHEMISTRY

EDGE ARTICLE

View Article Online
View Journal

Cite this: DOI: 10.1039/d5sc03828f

All publication charges for this article have been paid for by the Royal Society of Chemistry

Energy migration, charge transfer, and charge dissociation in self-assembling nonfullerene acceptor aggregates with zincporphyrin-nonfullerene acceptor dyads†

Yasunari Tamai, *[ab] Midori Akiyama, [c] Lorenzo Vallan, [c] Daiki Sasada,[c] Katsuaki Suzuki,[d] Hironori Kaji, *[d] Takumi Urakami,[c] Hirofumi Sato, [c] Masahiro Higashi, *[e] Seiichiro Izawa, [f] Motohisa Kubota,[c] Tomokazu Umeyama [g] and Hiroshi Imahori *[chi]

The synergy between self-assembling donor–acceptor–donor type nonfullerene acceptors (**TACIC-Br**) and zincporphyrin-nonfullerene acceptor linked molecules (**ZnP-TACIC**) provides a compelling model for examining key multi-step processes, including energy migration, charge transfer (CT), and charge dissociation (CD) in photosynthesis and organic photovoltaics (OPVs). Remarkably, **TACIC-Br** molecules exhibited a strong tendency to aggregate, even in the good solvent $CHCl_3$. However, when the proportion of the poor solvent (MeOH) exceeded 40% in a $CHCl_3$/MeOH mixture (v/v), these aggregates displayed an unusually prolonged excited singlet-state lifetime, comparable to **TACIC**s in thin films. Solid-state NMR spectroscopy and theoretical calculations revealed that within the **TACIC** aggregates, a slipped or T-shaped dimeric π–π packing arrangement is favored, positioning the thienoazacoronene donor unit and the 1,1-dicyanomethylene-3-indanone acceptor unit in close proximity. This supramolecular packing effectively suppresses both nonradiative and radiative decay processes in $CHCl_3$/MeOH mixtures and thin films, contrasting sharply with typical self-quenching observed in conventional dye aggregates. Time-resolved transient absorption measurements showed efficient energy migration, CT, and CD within these composite aggregates. With an extremely long singlet excited-state diffusion length (L_D) of 45.6 nm, facilitated by the prolonged excited singlet-state lifetime, **TACIC**s are well-suited for efficient energy migration. Notably, after quantitative CT at the **ZnP-TACIC** molecule, 35% of the CT states in the aggregates dissociated to form free ion pairs. This integrated supramolecular approach adeptly emulates both light-harvesting and CT and CD processes in photosynthesis and OPVs, thereby offering potential applications in solar energy conversion.

Received 27th May 2025
Accepted 23rd July 2025

DOI: 10.1039/d5sc03828f

rsc.li/chemical-science

Introduction

Supramolecular chemistry investigates intermolecular bonds such as hydrogen bonding, π–π interactions, and electrostatic forces. This field focuses on understanding the structures and functions of the assemblies formed through interactions between two or more complex chemical species.[1] The overarching goal is to develop molecular and supramolecular devices, which are integrated chemical systems with organized structures and specialized functions built upon supramolecular architectures.[2–14] However, constructing supramolecular

[a]Department of Advanced Materials Science, Graduate School of Frontier Sciences, The University of Tokyo, Kashiwanoha 5-1-5, Kashiwa, 277-8561, Japan. E-mail: tamai@edu.k.u-tokyo.ac.jp

[b]Japan Science and Technology Agency (JST), PRESTO, 4-1-8 Honcho, Kawaguchi, Saitama, 332-0012, Japan

[c]Department of Molecular Engineering, Graduate School of Engineering, Kyoto University, Kyoto, 615-8510, Japan. E-mail: imahori@scl.kyoto-u.ac.jp

[d]Institute for Chemical Research, Kyoto University, Uji, Kyoto, 611-0011, Japan. E-mail: kaji@scl.kyoto-u.ac.jp

[e]Department of Complex Systems Science, Graduate School of Informatics, Nagoya University, Furo-cho, Chikusa-ku, Nagoya, 464-8601, Japan. E-mail: higashi@nagoya-u.jp

[f]Materials and Structures Laboratory, Institute of Science Tokyo, 4259 Nagatsuta-cho, Midori-ku, Yokohama, Kanagawa, 226-8503, Japan

[g]Department of Applied Chemistry, Graduate School of Engineering, University of Hyogo, Himeji, Hyogo, 671-2280, Japan

[h]Institute for Integrated Cell-Material Sciences (WPI-iCeMS), Kyoto University, Kyoto, 606-8501, Japan

[i]Institute for Liberal Arts and Sciences (ILAS), Kyoto University, Kyoto, 606-8316, Japan

† Electronic supplementary information (ESI) available. See DOI: https://doi.org/10.1039/d5sc03828f

systems with enhanced, multifaceted functionality poses a challenge due to the inherent weakness and complexity of these interactions. When self-assembling units are deliberately introduced into molecules, they may promote organization, yet this often compromises the intended functions due to interference from the rather bulky self-assembling units. Therefore, the ideal approach involves embedding self-assembling units directly into molecular frameworks without hindering functional properties.

A compelling area within supramolecular chemistry is light energy conversion.[15–30] Photosynthesis serves as inspiration, where sunlight is captured by precisely arranged chromophores in light-harvesting complexes. The collected energy is directed to reaction centers for charge separation (CS), transforming light into chemical energy. Mimicking this natural multi-step processes, supramolecular strategies have been employed to integrate energy transduction and CS in both solutions and electrodes.[15–37] These methods have demonstrated potential for efficiently converting light energy into chemical energy in solar fuels generation and electricity in organic photovoltaics (OPVs).

Nonfullerene acceptors (NFAs) have gathered considerable attention due to their high light-harvesting properties in the visible and near-infrared region, facile HOMO–LUMO level tuning, and self charge transfer (CT) and charge dissociation (CD) at interfaces of OPVs, improving power conversion efficiencies (PCEs) of up to 20%.[38–40] Recently, we introduced a new class of NFAs, termed **TACIC** (X = H in Fig. 1), specifically designed for OPVs.[41–43] The OPV device with PBDB-T donor polymer and **TACIC** showed a PCE of 9.92%, which was comparable to a PCE (9.71%) of the OPV device with PBDB-T and the representative NFA, ITIC (*vide infra*).[41] Given the self-assembling characteristics of thienoazacoronene through π–π interactions,[44–46] we hypothesized that integrating this moiety into the donor moiety of acceptor–donor–acceptor (A–D–A) type NFAs would strengthen intermolecular interactions, positively impacting photodynamics. Indeed, **TACIC** stands apart from conventional NFAs including ITIC, exhibiting an extended excited singlet-state lifetime in thin films (τ = 1.3–2.3 ns) compared to chloroform solution (≤0.22 ns). This distinct behavior stems from its intrinsic self-assembly, which effectively reduces both radiative (k_r) and nonradiative (k_{nr}) decay rate constants in films. Importantly, this self-assembly is an inherent feature of its molecular structure, preserving its core photophysical properties despite the yet-to-be-elucidated supramolecular structures of **TACIC** due to its amorphous state. It should be emphasized here that the prolonged excited singlet state of NFAs enables a reduced driving force for photoinduced charge transfer (CT) from donor polymers to NFAs, thereby minimizing open-circuit voltage loss and enhancing PCE in OPVs.[38–40] We hypothesized that if **TACIC** aggregates in solutions could form structures akin to those in films, efficient energy migration within the aggregates would ensure. More importantly, integrating D–A molecules capable of CS within these aggregates would enable energy migration to facilitate CT and CD.

In this study, we designed a **TACIC-Br** (X = Br in Fig. 1) and a zincporphyrin (ZnP)-**TACIC** dyad (Fig. 1). **TACIC-Br** is expected to aggregate in solution due to its structural similarity to **TACIC**. Meanwhile, ZnP acts as an excellent electron donor for photoinduced electron transfer (ET),[17,29,30] and ET from ZnP to the excited singlet state (S_1) of **TACIC** is anticipated based on their optical and electrochemical properties.[30,41] First, we fully characterized the supramolecular aggregates of **TACIC-Br** using spectroscopic measurements and theoretical calculations. Subsequently, **ZnP-TACIC** molecules were incorporated into **TACIC-Br** aggregates in solution, and their photodynamics were analyzed using time-resolved transient absorption (TA) spectroscopy. Our results revealed efficient energy migration, CT, and CD within the aggregates. This is highlighted by an extraordinary singlet excited-state diffusion length (L_D) of 45.6 nm originating from the long-lived excited singlet state in the aggregates, surpassing those of typical organic semiconductors (5–10 nm).[47–50]

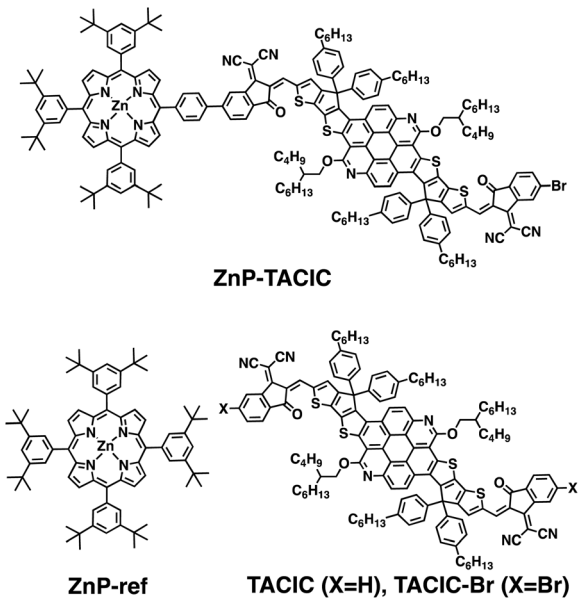

Fig. 1 Molecular structures of ZnP-TACIC, ZnP-ref, TACIC (X = H), and TACIC-Br (X = Br).

Results and discussion

Synthesis

The synthetic routes to **TACIC-Br** and **ZnP-TACIC** are illustrated in Schemes S1 and S2, and details of the synthesis are provided in the ESI.† Briefly, **TACIC-Br** was obtained by Knoevenagel condensation between the corresponding aldehyde[41] and (6-bromo-2,3-dihydro-3-oxo-1*H*-inden-1-ylidene)propanedinitrile.[51] **ZnP-TACIC** was synthesized by Stille coupling between the corresponding ZnP tin reagent[51,52] and **TACIC-Br**. **ZnP-ref** was also prepared.[53] The molecular structures were characterized by solution ^{1}H NMR spectroscopy (Fig. S1†), Fourier transfer infrared (FT-IR) spectroscopy (Fig. S2†), and high-resolution mass spectrometry (HRMS) (Fig. S3†).

Aggregation behavior of TACIC-Br

The aggregation behavior of **TACIC-Br** was examined in a mixture of $CHCl_3$ and MeOH (Fig. 2a). In the good solvent, $CHCl_3$, **TACIC-Br** displayed an absorption peak at 700 nm with a shoulder at 650 nm, which is similar to that of **TACIC**.[41] As the

ratio of the poor solvent, MeOH, increased, the band at 700 nm decreased, and a new peak emerged at 750 nm. Further increasing the MeOH ratio led to the formation of precipitates. Correspondingly, the fluorescence also exhibited a redshift with decreasing intensity (Fig. 2b). These behaviors suggest the formation of **TACIC-Br** aggregates in the mixed solvent.

The fluorescence lifetime of the **TACIC-Br** aggregates was measured in a mixture of $CHCl_3$ and MeOH (Table S1†). The sample was excited at 636 nm, with emission monitored at 750 nm. When the MeOH ratio ranged from 0–30%, the fluorescence lifetime (τ) remained nearly constant at 0.4–0.5 ns, displaying a single short-lived component (Fig. S4†). However, with MeOH ratios exceeding 40%, the average lifetime considerably increased due to the emergence of a long-lived component. Dynamic light scattering measurements revealed the formation of **TACIC-Br** aggregates with mean diameters (D_M) between 10–15 nm regardless of the $CHCl_3$ to MeOH ratio (Fig. S5†). Based on trends in the UV-visible-NIR absorption spectra, steady-state fluorescence spectra, fluorescence lifetimes, and aggregate sizes as a function of the MeOH ratio, we proposed a plausible formation mechanism for the **TACIC-Br** aggregates. Within the $CHCl_3$: MeOH ratios of 100 : 0 to 60 : 40 (v/v), aggregates of D_M = 10–15 nm with a fluorescence lifetime of 0.4–0.5 ns are formed, but the aggregated states are largely comparable. As the MeOH ratio increases further ($CHCl_3$: MeOH = 60 : 40 to 40 : 60), a dramatic change in the aggregated state occurs, while maintaining a similar size, thereby prolonging the average fluorescence lifetime from 0.4–0.5 ns to 2.3 ns, which is close to the aggregated states of **TACIC** (τ = 1.6 ns),[41] **TACIC-Br** (τ = 1.9 ns), and **TACIC** derivatives (τ = 1.3–2.3 ns)[42] in films. For the subsequent time resolved TA experiments, we fixed the solvent mixed ratio at 50 : 50, reflecting the representative **TACIC-Br** aggregates with an extended fluorescence lifetime (*vide infra*).

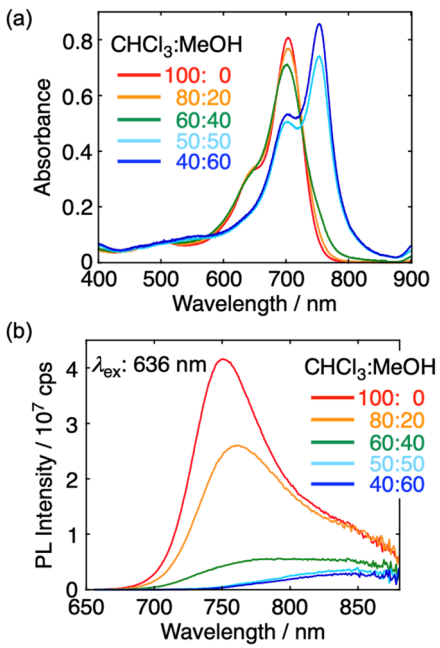

Fig. 2 (a) UV-vis-NIR absorption spectra and (b) fluorescence spectra of **TACIC-Br** in a mixture of $CHCl_3$ and MeOH (1×10^{-5} M). The inset depicts the ratio of $CHCl_3$: MeOH (v/v).

To further examine the intermolecular interactions within the aggregates, solid-state NMR (ssNMR) spectroscopy was performed on **TACIC** (X = H) as a reference for **TACIC-Br**. One-dimensional (1D) ^{1}H magic angle spinning (MAS) and ^{13}C cross-polarization (CP)/MAS spectra of **TACIC** are presented in Fig. S6 and S7,† respectively. In the 1D ^{1}H MAS spectrum, peaks observed at −1 to 3 ppm, 5 ppm, and 6–10 ppm were attributed to protons in different environments: alkyl and alkoxy side chains (H_aliphatic), α-carbon of the alkoxy side chain on the thienoazacoronene unit (H1), and the π-conjugated unit (H2–H11) within the aggregates, respectively. A detailed assignment is provided in Fig. S6.† While the 1D ^{13}C CP/MAS spectra exhibited significant signal overlap, some peaks (C1, C2, C3, C4, and C5) could be distinctly assigned with the aid of DFT chemical shift calculations, as shown in Fig. S7.†

Further insight into the intermolecular packing was gained from a two-dimensional (2D) ^{1}H–^{13}C heteronuclear correlation (HETCOR) spectrum which identifies spatially proximate ^{1}H–^{13}C spin pairs. Weak correlations were detected between the ^{13}C peak at 68.5 ppm and 115 ppm and the ^{1}H peak near 5.0 ppm, corresponding to H1/C3 and H1/C4 pairs (Fig. 3a, red circles). Given that the intramolecular distances of H1/C3 and H1/C4 exceed 10 Å in the DFT-optimized structure, these cross peaks were attributed to intermolecular correlation. These findings suggest that within the amorphous **TACIC** aggregate, a slipped or T-shaped dimeric π–π packing arrangement is preferred (see the next theoretical calculation section), wherein the thienoazacoronene unit and the 1,1-dicyanomethylene-3-indanone acceptor unit are positioned in close proximity (Fig. 3b). Such π–π packing rationalizes the suppressed non-radiative decay of **TACIC** in the aggregates formed within the mixed solvents and in thin films ($k_{nr} = 5.8 \times 10^8$ s^{-1}) compared to its behavior in pure chloroform ($k_{nr} = 4.2 \times 10^9$ s^{-1}).[41]

To further explore intermolecular interactions, theoretical calculations were conducted, with computational details provided in the ESI.† First, molecular dynamics (MD) simulations were performed to investigate the stacking structures of **TACIC** in the film state. The results revealed that two π–π packing conformations are nearly equally dominant: the slipped structure, where the acceptor moieties overlap, and the T-shaped structure, where the acceptor and donor moieties overlap (Fig. S8†). This finding aligns with the ssNMR results discussed earlier. Notably, this contrasts with ITIC, a representative NFA, where only the slipped structure is predominant.[39]

Next, the time-dependent density functional theory (TDDFT) calculations were employed to examine the fluorescent properties of the **TACIC** monomer and its slipped and T-shaped π–π packing dimers. The S_1 fluorescent states of the **TACIC** monomer and dimers are primarily characterized by the HOMO–LUMO transitions. In the monomer, the HOMO and LUMO are delocalized across the entire molecule, resulting in a large transition dipole strength (Fig. 4). However, in **TACIC** dimers, the transition dipole strengths are significantly reduced because the HOMO and LUMO are separated and localized

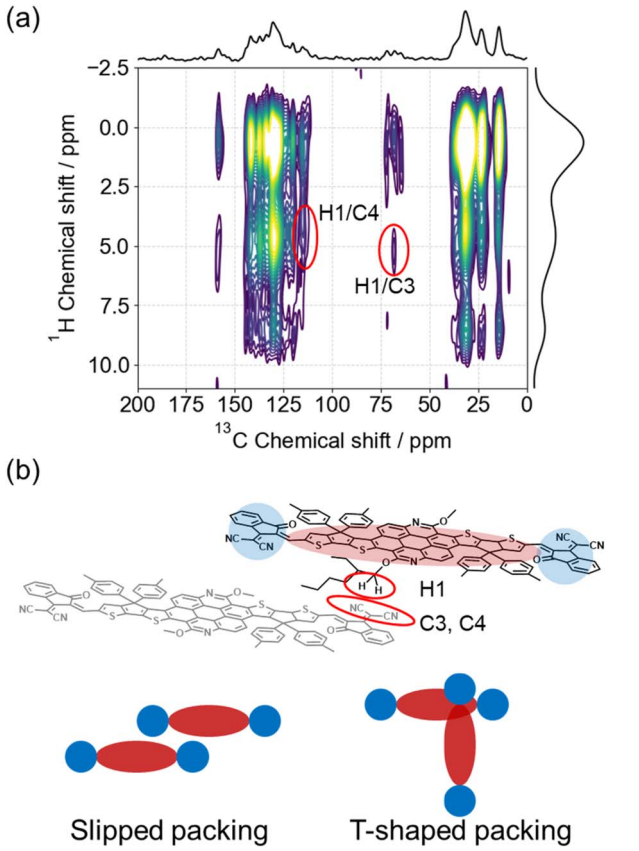

Fig. 3 (a) 2D ^{1}H–^{13}C HETCOR ssNMR spectrum of **TACIC** and (b) expected aggregated structures.

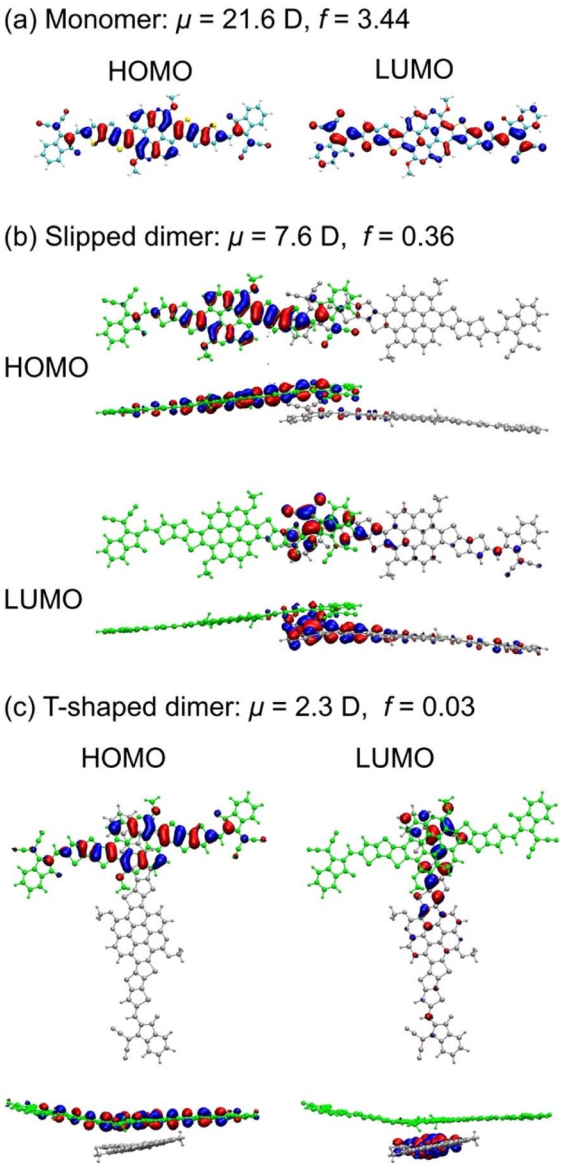

Fig. 4 Calculated transition dipole strength (μ), oscillator strength (f), HOMO and LUMO (isovalue = 0.02) of (a) **TACIC** monomer, (b) slipped dimer, and (c) T-shaped dimer at the S_1 optimized geometry. The phenyl sidechains are omitted for simplicity.

significantly on the overlapped moieties of respective monomers. The same trend was found for **TACIC-Br** (Fig. S9†). In contrast, the HOMO and LUMO of ITIC dimers are delocalized throughout the dimer, leading to an enhanced transition dipole moment strength (Fig. S10†). These theoretical results are consistent with the experimental results of radiative rate constants (k_r); the k_r of **TACIC** in the film state (4.8×10^7 s^{-1}) is smaller than in pure chloroform (3.0×10^8 s^{-1}), whereas the k_r of ITIC in the film state (7.5×10^8 s^{-1}) is larger than in the solution (3.6×10^8 s^{-1}).[41]

Optical properties of ZnP-TACIC

The UV-vis-NIR absorption spectra of **ZnP-TACIC**, **TACIC-Br**, and **ZnP-ref** were measured in benzonitrile (PhCN), which has a dielectric constant of 26, close to the estimated value of the $CHCl_3$: MeOH mixed solvent (50 : 50, v/v) (19). The absorption spectrum of **ZnP-TACIC** is almost a linear combination of those of **ZnP-ref** and **TACIC-Br**, indicating negligible interaction between the ZnP and **TACIC** units in the ground state (Fig. 5a). The fluorescence spectra of **ZnP-TACIC** and **TACIC-Br** were recorded in PhCN, with the **TACIC-Br** moiety selectively excited at 690 nm (Fig. 5b). The fluorescence of **ZnP-TACIC** is significantly quenched compared to that of **TACIC-Br**, suggesting the occurrence of photoinduced ET from ZnP to the **TACIC-Br** excited singlet-state (S_1). This is consistent with the exothermic driving forces for CS (0.42 eV) and charge recombination (CR) (1.28 eV) in **ZnP-TACIC** in benzonitrile, based on the first oxidation potential of ZnP (0.32 V *vs.* Fc/Fc$^+$), the first reduction potential of **TACIC** (−0.96 V *vs.* Fc/Fc$^+$), and the optical HOMO–LUMO gap (1.70 eV) of **TACIC**.[41]

Additive effects of ZnP-TACIC

We examined the additive effects of **ZnP-TACIC** on the optical properties of the **TACIC** aggregates. The ratio of $CHCl_3$: MeOH (50 : 50, v/v) was fixed (*vide supra*), while the molar ratio of **TACIC-Br** : **ZnP-TACIC** was varied. Upon adding the **ZnP-TACIC** solution to the **TACIC-Br** aggregate solution, a slight decrease in the **TACIC-Br** absorption at 700 and 750 nm, as well as a slight

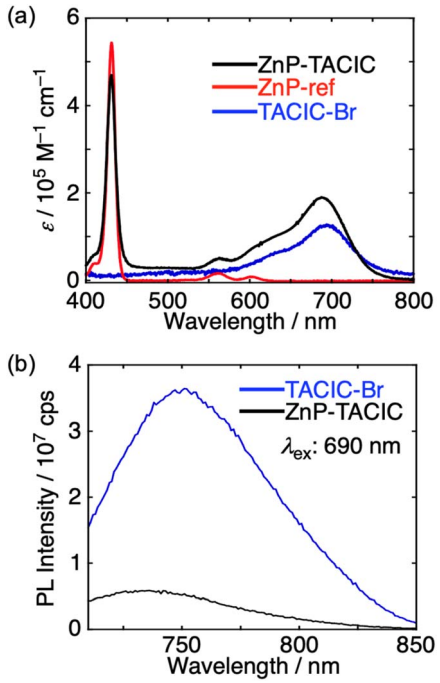

Fig. 5 (a) UV-vis-NIR absorption spectra of ZnP-TACIC, ZnP-ref, and TACIC-Br in benzonitrile. (b) Fluorescence spectra of TACIC-Br and ZnP-TACIC in benzonitrile.

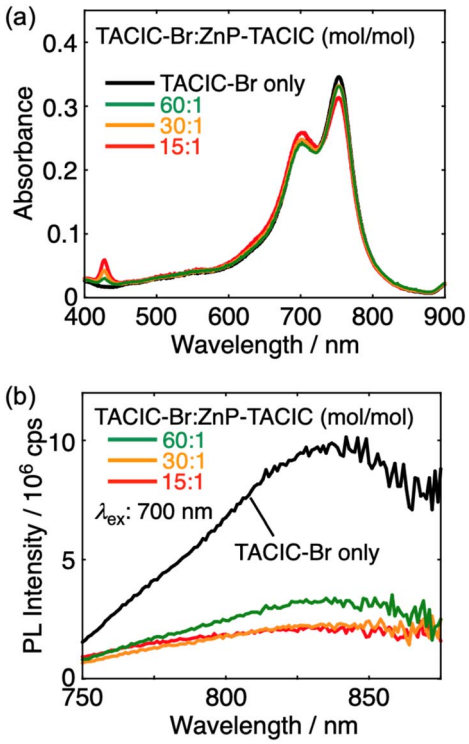

Fig. 6 (a) UV-vis-NIR absorption spectra and (b) fluorescence spectra of TACIC-Br/ZnP-TACIC in a mixture of $CHCl_3$ and MeOH (1×10^{-5} M, 50 : 50, v/v). The inset depicts the molar ratio of TACIC-Br : ZnP-TACIC.

increase in the ZnP absorption, was observed (Fig. 6a). Meanwhile, the fluorescence of **TACIC-Br** at 830 nm was significantly quenched with a molar ratio of up to 60 : 1 when the **TACIC-Br** moiety was excited solely at 700 nm (Fig. 6b). These results suggest that **ZnP-TACIC** is incorporated into the **TACIC-Br** aggregates (denoted as **TACIC-Br/ZnP-TACIC**), and efficient energy migration in the **TACIC-Br/ZnP-TACIC** aggregates and subsequent CS in **ZnP-TACIC** occur when a small molar ratio of **ZnP-TACIC** is added to the **TACIC-Br** aggregate solution.

From the dynamic light scattering experiments, the size of the **TACIC-Br** aggregates appears to decrease slightly as the MeOH ratio in $CHCl_3$ increases (Fig. S5†). However, this trend is not consistent, and we are therefore unable to evaluate the effect of **ZnP-TACIC** as an additive. To investigate the impact of mixing order on aggregate formation, we conducted the following experiments: Order A: (1) a $CHCl_3$ solution of **ZnP-TACIC** was added to a $CHCl_3$ solution of **TACIC-Br** to achieve a molar ratio of **TACIC-Br : ZnP-TACIC** = 10 : 1. (2) MeOH was then added to adjust the solvent ratio to $CHCl_3$: MeOH = 50 : 50. Order B: (1) MeOH was added to a $CHCl_3$ solution of **TACIC-Br** to reach a solvent ratio of approximately $CHCl_3$: MeOH = 50 : 50. (2) A $CHCl_3$ solution of **ZnP-TACIC** was then added to achieve a final molar ratio of **TACIC-Br : ZnP-TACIC** = 10 : 1 while maintaining the $CHCl_3$: MeOH ratio at approximately 50 : 50. In both cases, selective excitation of **TACIC-Br** resulted in pronounced fluorescence quenching, indicating that energy migration and charge transfer processes occur efficiently regardless of the **ZnP-TACIC** incorporation sequence in the **TACIC-Br** aggregates.

Transient absorption measurements

The time-resolved TA measurements were performed for **TACIC-Br** and **ZnP-TACIC** in $CHCl_3$. Upon excitation at 700 nm, positive absorptions arising from the S_1 state at 600 and 1100 nm, as well as negative ground-state bleaching at 700 nm, were observed for **TACIC-Br** (Fig. 7a). A similar absorption profile was noted for **TACIC**.[41] The absorption decayed with a time constant of 410 ps (Fig. S11a†), which agreed with the fluorescence lifetime of **TACIC-Br** (τ = 438 ps). For **ZnP-TACIC**, the absorptions decayed faster than those in **TACIC-Br**, suggesting the occurrence of photoinduced ET from ZnP to the S_1 state of **TACIC** (Fig. 7b). Indeed, as the S_1 absorption decayed, characteristic ground-state bleaching at 420 nm, arising from ZnP radical cation ($ZnP^{\bullet+}$), and positive absorption at 750 nm, arising from **TACIC** radical anion (**TACIC**$^{\bullet-}$), emerged.[41] Given the spectral overlap between **TACIC**$^{\bullet-}$ and the ground-state bleaching and considering the intrinsic synchronization of radical cation and anion dynamics, the charge dynamics were analyzed using the 420 nm signal, which exhibits minimal spectral overlap. From the absorption profile fitting, the CS and CR time constants of 8.8 ps and 140 ps were obtained (Fig. S11b†). Taking into account the fluorescence lifetime of **TACIC-Br**, the charge separation efficiency approaches unity.

The time-resolved TA measurements were also conducted for the **TACIC-Br/ZnP-TACIC** aggregates with a molar ratio of **TACIC-Br : ZnP-TACIC** (10 : 1) in a mixture of $CHCl_3$ and MeOH

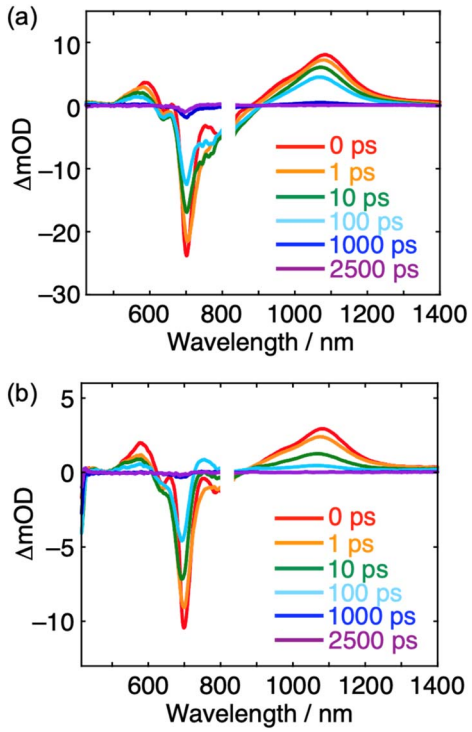

Fig. 7 Femtosecond time-resolved transient absorption spectra of (a) TACIC-Br and (b) ZnP-TACIC in $CHCl_3$ (3×10^{-5} M). The inset depicts the delay time after excitation at 700 nm.

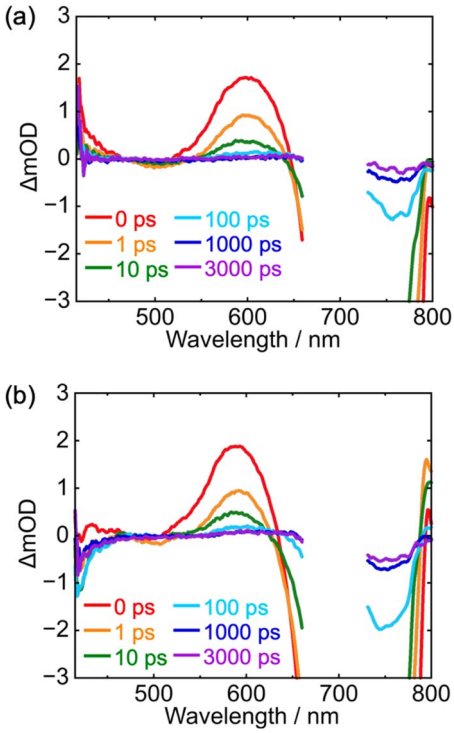

Fig. 8 Femtosecond time-resolved transient absorption spectra of (a) TACIC-Br and (b) TACIC-Br/ZnP-TACIC with a molar ratio of 10 : 1 in a mixture of $CHCl_3$ and MeOH (50 : 50, v/v, 1×10^{-5} M of TACIC-Br). The inset depicts the delay time after excitation at 700 nm. Strong scattering of the excitation pump pulse by aggregates obscures the wavelength region around 700 nm. The vertical axis has been expanded to better visualize the S_1 state and $TACIC^{\bullet -}$. The complete intense ground-state bleaching signal up to its peak is presented in Fig. S12.†

(50 : 50, v/v). In the subsequent measurements, we focused on the visible region due to its information richness. Upon excitation at 700 nm, positive absorption arising from the S_1 state of **TACIC-Br** at 600 nm was observed for the **TACIC-Br** aggregates in both the absence and presence of **ZnP-TACIC** (Fig. 8). In the aggregated state, the ground-state bleaching (as well as the steady-state absorption) of **TACIC-Br** exhibits a red shift relative to that in solution, leading to increased spectral overlap with $TACIC^{\bullet -}$. Consequently, the relatively weak absorption of $TACIC^{\bullet -}$ is masked by the intense ground-state bleaching. However, in the presence of **ZnP-TACIC**, a positive absorption at 800 nm, attributable to the absorption tail of $TACIC^{\bullet -}$, and the characteristic ground-state bleaching at 420 nm, arising from $ZnP^{\bullet +}$, were detected. This supports the formation of the charge-separated state for the **TACIC-Br/ZnP-TACIC** aggregates. As in the solution systems, the ground-state bleaching signal at 420 nm, derived from $ZnP^{\bullet +}$ with minimal spectral overlap, was employed in the subsequent decay analysis.

To determine whether energy transfer from **TACIC-Br** molecules near **ZnP-TACIC** or energy migration among the **TACIC-Br** aggregate contributes to CS, the excitation intensity dependence of TA spectra was investigated. As the excitation intensity at 700 nm increased, CS took place more rapidly in the **TACIC-Br/ZnP-TACIC** aggregates with a molar ratio of **TACIC-Br : ZnP-TACIC** (10 : 1) in a mixture of $CHCl_3$ and MeOH (50 : 50, v/v) (Fig. 9 and S12†). This suggests that the S_1 state of **TACIC-Br** far from **ZnP-TACIC** does not contribute to CS due to the fast relaxation of the S_1 state by singlet-singlet annihilation. However, under the weak excitation intensity (<5 μJ cm^{-2}), the CS rate constant slows down, exceeding the CS rate constant of **ZnP-TACIC** in $CHCl_3$ (8.8 ps). These results demonstrate that CS is regulated by diffusion-controlled singlet excited-state migration. Under the excitation intensity of 18.7 μJ cm^{-2}, the CR rate constant of 260 ps is longer than that of **ZnP-TACIC** in $CHCl_3$ (140 ps). We underscore that approximately 35% of the charge-separated state in the aggregates persisted on a nanosecond timescale, in stark contrast to those in **ZnP-TACIC** in $CHCl_3$, where the charge-separated state decayed completely within 1 ns. These results indicate that a fraction of $TACIC^{\bullet -}$ diffuse through the aggregates opposing the Coulomb attraction, thereby preventing CR.

The singlet excited-state diffusion length (L_D) of **TACIC-Br** was determined to be 45.6 nm (Fig. S13†). Given the L_D value and the singlet excited-state lifetime of 2.2 ns, diffusion coefficient (D) was calculated to be 9.5×10^{-3} cm^2 s^{-1}. This value is lower than that of ITIC-Cl (2.7×10^{-2} cm^2 s^{-1}),[54] which we previously determined using the same methodology. Considering $\tau = 140$ ps for ITIC-Cl, the L_D value of **TACIC-Br** is 2.4 times higher than that of ITIC-Cl, demonstrating the potential utility of the **TACIC** structure for efficient energy migration.

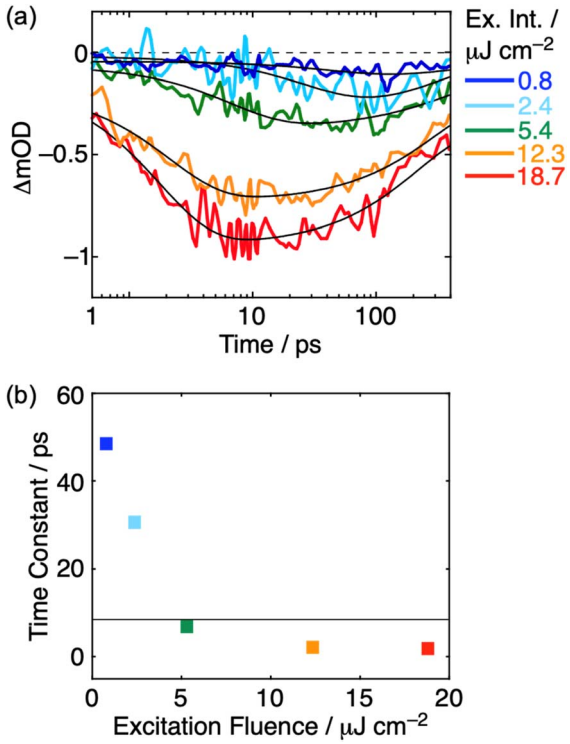

Fig. 9 (a) Excitation intensity dependence of ground-state bleaching formation corresponding to $ZnP^{\bullet+}$ (averaged over 420–430 nm) and (b) plot of CS rate constant as a function of excitation fluence at 700 nm. The molar ratio of **TACIC-Br**/**ZnP-TACIC** aggregates is 10 : 1 and the ratio of $CHCl_3$ and MeOH is 50 : 50 (v/v). The inset depicts the excitation intensity. The black lines in panel (a) represent the best fitting curves of the transient absorption data with bi-exponential functions and a constant offset. The horizontal line in panel (b) represents the CS rate constant of **ZnP-TACIC** in $CHCl_3$ (8.8 ps) as a guide for the eye.

Experimental

Experimental details including materials, methods, synthetic procedures, solution ^{1}H NMR spectra, IR spectra, mass spectra, optical measurements, DLS measurements, solid-state ^{1}H and ^{13}C NMR spectra, MD and TDDFT calculations, TA measurements, and the details of determination of L_D are provided in the ESI.†

Conclusions

The dynamic interplay between the self-assembling non-fullerene acceptor **TACIC-Br** and the zincporphyrin (ZnP)-**TACIC** dyad presents a fascinating model for emulating energy transduction and charge separation, akin to natural photosynthesis and organic photovoltaics. Notably, **TACIC-Br** molecules exhibit a strong tendency to aggregate even in the favorable solvent $CHCl_3$. However, when the proportion of the poor solvent (MeOH) surpasses 40% in a $CHCl_3$/MeOH mixture (v/v), these aggregates exhibit an extended singlet-state lifetime, comparable to **TACIC** thin films. Solid-state NMR spectroscopy and theoretical calculations showed for the first time the importance of dimeric π–π packing structures for the unusual photophysical properties of **TACIC** aggregates: within these aggregates, a slipped or T-shaped dimeric π–π packing arrangement is favored, bringing the thienoazacoronene donor unit and the 1,1-dicyanomethylene-3-indanone acceptor unit into close proximity. This supramolecular π–π packing effectively minimizes both nonradiative and radiative decay processes, shaping the unique photophysical behavior of **TACIC** in chloroform/MeOH mixtures and thin films, in contrast to its behavior in pure chloroform. Such relationship between molecular structure, packing structure, and photophysical properties of NFAs are pivotal for rational molecular design of photoactive organic functional molecules in solid states.

In $CHCl_3$/MeOH mixtures exceeding 40% MeOH, **TACIC-Br**/**ZnP-TACIC** aggregates exhibit substantial fluorescence quenching of **TACIC-Br** by **ZnP-TACIC**, even at a **TACIC-Br : ZnP-TACIC** molar ratio of up to 30 : 1. Time-resolved transient absorption measurements highlighted efficient energy migration and charge separation within these aggregates, demonstrating an extraordinarily long singlet excited-state diffusion length (L_D) of 45.6 nm due to the prolonged excited singlet state lifetime—far exceeding the typical 5–10 nm range observed in organic semiconductors and ranking among the longest diffusion lengths reported for recently developed novel NFAs. Remarkably, after quantitative charge-transfer at the charge separation molecule, approximately 35% of the charge-separated states within these aggregates successfully dissociate, forming free ion pairs as the **TACIC** radical anion fraction diffuses and overcomes Coulomb attraction. This integrated supramolecular strategy adeptly replicates both light-harvesting and charge separation mechanisms (including charge transfer and charge dissociation) observed in photosynthesis and organic photovoltaics. It holds promise for driving future advancements in artificial photosynthesis, solar fuels, and organic photovoltaics.

Data availability

The data supporting this article have been included as part of the ESI.†

Author contributions

H. Imahori conceived and designed this work. D. Sasada, M. Kubota, and T. Umeyama conducted the synthesis and characterization of the products. M. Akiyama and L. Vallan performed spectroscopic measurements. Y. Tamai and S. Izawa conducted TA and diffusion length measurements. K. Suzuki and H. Kaji performed solid-sate NMR measurements. T. Urakami, H. Sato, and M. Higashi carried out theoretical calculations. Y. Tamai, M. Akiyama, and H. Imahori co-wrote the manuscript.

Conflicts of interest

There are no conflicts to declare.

Acknowledgements

This work was supported by a Grant-in-Aid for Transformative Research Areas (A) (Dynamic Exciton: 20H05831, 20H05832, 20H05837, 20H05840, 21H05394, 23H03951), and Scientific Research (A) (24H00485), and JST PRESTO program (JPMJPR23J7), JSPS Core-to-Core Program (JPJSCCA20220004), and JST CREST (JPMJCR2431).

Notes and references

1 J.-M. Lehn, *Angew. Chem., Int. Ed.*, 1988, **27**, 89.
2 K. Ariga, Y. Yamauchi, G. Rydzek, Q. Ji, Y. Yonamine, K. C.-W. Wu and J. P. Hill, *Chem. Lett.*, 2014, **43**, 36.
3 A. Harada, Y. Takashima and M. Nakahata, *Acc. Chem. Res.*, 2014, **47**, 2128.
4 S. J. Barrow, S. Kasera, M. J. Rowland, J. del Barrio and O. A. Scherman, *Chem. Rev.*, 2015, **115**, 12320.
5 T. R. Cook and P. J. Stang, *Chem. Rev.*, 2015, **115**, 7001.
6 A. J. McConnell, C. S. Wood, P. P. Neelakandan and J. R. Nitschke, *Chem. Rev.*, 2015, **115**, 7729.
7 J.-P. Sauvage, *Angew. Chem., Int. Ed.*, 2017, **56**, 11080.
8 Z. Liu, S. K. M. Nalluri and J. F. Stoddart, *Chem. Soc. Rev.*, 2017, **46**, 2459.
9 I. V. Kolesnichenko and E. V. Anslyn, *Chem. Soc. Rev.*, 2017, **46**, 2385.
10 S. P. Black, J. K. M. Sanders and A. R. Stefankiewicz, *Chem. Soc. Rev.*, 2014, **43**, 1861.
11 D. B. Amabilino, D. K. Smith and J. W. Steed, *Chem. Soc. Rev.*, 2017, **46**, 2404.
12 T. Ogoshi, T. Kakuta and T. Yamagishi, *Angew. Chem., Int. Ed.*, 2019, **58**, 2197.
13 J. Li, J. Wang, H. Li, N. Song, D. Wang and B. Z. Tang, *Chem. Soc. Rev.*, 2020, **49**, 1144.
14 C. Guo, A. C. Sedgwick, T. Hirao and J. L. Sessler, *Coord. Chem. Rev.*, 2021, **427**, 213560.
15 M. R. Wasielewski, *Chem. Rev.*, 1992, **92**, 435.
16 J. H. Alstrum-Acevedo, M. K. Brennaman and T. J. Meyer, *Inorg. Chem.*, 2005, **44**, 6802.
17 H. Imahori, *Bull. Chem. Soc. Jpn.*, 2007, **80**, 621.
18 D. Gust, T. A. Moore and A. L. Moore, *Acc. Chem. Res.*, 2009, **42**, 1890.
19 A. Magnuson, M. Anderlund, O. Johansson, P. Lindblad, R. Lomoth, T. Polivka, S. Ott, K. Stensjö, S. Styring, V. Sundström and L. Hammarström, *Acc. Chem. Res.*, 2009, **42**, 1899.
20 M. R. Wasielewski, *Acc. Chem. Res.*, 2009, **42**, 1910.
21 N. Aratani, D. Kim and A. Osuka, *Acc. Chem. Res.*, 2009, **42**, 1922.
22 P. D. Frischmann, K. Mahata and F. Würthner, *Chem. Soc. Rev.*, 2013, **42**, 1847.
23 S. Fukuzumi and K. Ohkubo, *Org. Biomol. Chem.*, 2014, **12**, 6059.
24 M. Rudolf, S. V. Kirner and D. M. Guldi, *Chem. Soc. Rev.*, 2016, **45**, 612.
25 C. B. KC and F. D'Souza, *Coord. Chem. Rev.*, 2016, **322**, 104.
26 Y. Pellegrin and F. Odobel, *C. R. Chim.*, 2017, **20**, 283.
27 B. Zhang and L. Sun, *Chem. Soc. Rev.*, 2019, **48**, 2216.
28 H. Kumagai, Y. Tamaki and O. Ishitani, *Acc. Chem. Res.*, 2022, **55**, 978.
29 H. Imahori, *Bull. Chem. Soc. Jpn.*, 2023, **96**, 339.
30 H. Imahori and M. Akiyama, *J. Porphyrins Phthalocyanines*, 2024, **28**, 319.
31 H. Imahori, H. Norieda, H. Yamada, Y. Nishimura, I. Yamazaki, Y. Sakata and S. Fukuzumi, *J. Am. Chem. Soc.*, 2001, **123**, 100.
32 W.-S. Li, K. S. Kim, D.-L. Jian, H. Tanaka, T. Kawai, J. H. Kwon, D. Kim and T. Aida, *J. Am. Chem. Soc.*, 2006, **128**, 10527.
33 Y. Kuramochi, A. S. D. Sandanayaka, A. Satake, Y. Araki, K. Ogawa, O. Ito and Y. Kobuke, *Chem.–Eur. J.*, 2009, **15**, 2317.
34 K. Börjesson, J. Tumpane, T. Ljungdahl, L. M. Wilhelmsson, B. Nordén, T. Brown, J. Mårtensson and B. Albinsson, *J. Am. Chem. Soc.*, 2009, **131**, 2831.
35 T. Miura, R. Tao, S. Shibata, T. Umeyama, T. Tachikawa, H. Imahori and Y. Kobori, *J. Am. Chem. Soc.*, 2016, **138**, 5879.
36 J. Otsuki, T. Okumura, K. Sugawa, S. Kawano, K. Tanaka, T. Hirao, T. Haino, Y. J. Lee, S. Kang and D. A. Kim, *Chem.–Eur. J.*, 2021, **27**, 4053.
37 J. Royakkers, H. Yang, A. J. Gillett, F. Eisner, P. Ghosh, D. G. Congrave, M. Azzouzi, Z. Andaji-Garmaroudi, A. Leventis, A. Rao, J. M. Frost, J. Nelson and H. Bronstein, *Nat. Chem.*, 2024, **16**, 1453.
38 G. C. Zhang, F. R. Lin, F. Qi, T. Heumüller, A. Distler, H. J. Egelhaaf, N. Li, P. C. Y. Chow, C. J. Brabec, A. K. Y. Jen and H. L. Yip, *Chem. Rev.*, 2022, **122**, 14180.
39 A. Yamakata, K. Kato, T. Urakami, S. Tsujimura, K. Murayama, M. Higashi, H. Sato, Y. Kobori, T. Umeyama and H. Imahori, *Chem. Sci.*, 2024, **15**, 12686.
40 H. Imahori, Y. Kobori and H. Kaji, *Acc. Mater. Res.*, 2021, **2**, 501.
41 T. Umeyama, K. Igarashi, D. Sasada, Y. Tamai, K. Ishida, T. Koganezawa, S. Ohtani, K. Tanaka, H. Ohkita and H. Imahori, *Chem. Sci.*, 2020, **11**, 3250.
42 T. Umeyama, K. Igarashi, D. Sasada, K. Ishida, T. Koganezawa, S. Ohtani, K. Tanaka and H. Imahori, *ACS Appl. Mater. Interfaces*, 2020, **12**, 39236.
43 M. Kubota, T. Umeyama, W. Suzuki, T. Koganezawa, M. Akiyama and H. Imahori, *Bull. Chem. Soc. Jpn.*, 2025, **98**, uoae147.
44 B. He, A. B. Pun, L. M. Klivansky, A. M. McGough, Y. Ye, J. Zhu, J. Guo, S. J. Teat and Y. Liu, *Chem. Mater.*, 2014, **26**, 3920.
45 B. He, B. A. Zhang, F. Liu, A. Navarro, M. P. Fernández-Liencres, R. Lu, K. Lo, T. L. Chen, T. P. Russell and Y. Liu, *ACS Appl. Mater. Interfaces*, 2015, **7**, 20034.
46 B. He, J. Dai, D. Zherebetskyy, T. L. Chen, B. A. Zhang, S. J. Teat, Q. Zhang, L. Wang and Y. A. Liu, *Chem. Sci.*, 2015, **6**, 3180.
47 O. V. Mikhnenko, P. W. M. Blom and T.-Q. Nguyen, *Energy Environ. Sci.*, 2015, **8**, 1867.
48 Y. Firdaus, V. M. Le Corre, S. Karuthedath, W. Liu, A. Markina, W. Huang, S. Chattopadhyay, M. M. Nahid,

M. I. Nugraha, Y. Lin, A. Seitkhan, A. Basu, W. Zhang, I. McCulloch, H. Ade, J. Labram, F. Laquai, D. Andrienko, L. J. A. Koster and T. D. Anthopoulos, *Nat. Commun.*, 2020, **11**, 5220.

49 H. Wang, H. Chen, W. Xie, H. Lai, T. Zhao, Y. Zhu, L. Chen, C. Ke, N. Zheng and F. He, *Adv. Funct. Mater.*, 2021, **31**, 2100877.

50 Y. Tamai, *Aggregate*, 2022, **6**, e280.

51 D. M. Knoll, T. B. Wiesner, S. M. Marschner, Z. Hasssan, P. Weis, M. Kappes, M. Nieger and S. Bräse, *RSC Adv.*, 2019, **9**, 30541.

52 T. Umeyama, T. Hanaoka, J. Baek, T. Higashino, F. Abou-Chahine, N. V. Tkachenko and H. Imahori, *J. Phys. Chem. C*, 2016, **120**, 28337.

53 S. Takagi, T. K. Miyamoto and Y. Sasaki, *Bull. Chem. Soc. Jpn.*, 1986, **59**, 2371.

54 Y. Sakamoto, S. Izawa, H. Ohkita, M. Hiramoto and Y. Tamai, *Commun. Mater.*, 2022, **3**, 76.